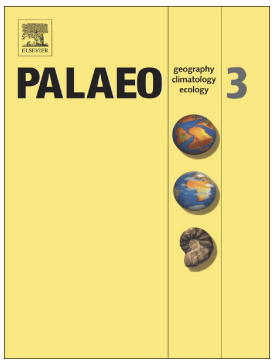

Reconstruction of temperature and monsoon precipitation in southwestern China since the last deglaciation

Xiaoshuang Sun, Can Zhang, Chengcheng Leng, Tianlong Yan

PII: S0031-0182(23)00609-0

DOI: https://doi.org/10.1016/j.palaeo.2023.111991

Reference: PALAEO 111991

To appear in: *Palaeogeography, Palaeoclimatology, Palaeoecology*

Received date: 15 November 2023

Revised date: 16 December 2023

Accepted date: 16 December 2023

Please cite this article as: X. Sun, C. Zhang, C. Leng, et al., Reconstruction of temperature and monsoon precipitation in southwestern China since the last deglaciation, *Palaeogeography, Palaeoclimatology, Palaeoecology* (2023), https://doi.org/10.1016/j.palaeo.2023.111991

Reconstruction of temperature and monsoon precipitation in southwestern China since the last deglaciation

Xiaoshuang Sun[a,b], Can Zhang[b*], Chengcheng Leng[c], Tianlong Yan[d]

a School of civil engineering and geomatics, Shandong University of Technology, Zibo 255000, Shandong, China

b State Key Laboratory of Lake Science and Environment, Nanjing Institute of Geography and Limnology, Chinese Academy of Sciences, Nanjing 210008, China

c School of Business, Shanghai Normal University Tianhua College, Shanghai 201825, China

d School of Geography, Liaoning Normal University, Dalian 116029, China

---

* Correspondence:

Can Zhang: czhang@niglas.ac.cn

Keywords: Southwestern China; mean annual temperature; monsoon precipitation; Last deglaciation and Holocene; GDGTs; alkane

Abstract:

Monsoon precipitation and temperature are the crucial components of the Indian monsoon climate, yet their spatial-temporal relationship remains unclear. In this study, we reconstruct the changes in monsoon precipitation and mean annual temperature simultaneously over the past 16,000 years using multiple proxies, including isoprenoid glycerol dialkyl glycerol tetraethers (isoGDGTs) and *n*-alkanes, from an alpine lake in southwestern China. On the one hand, the reconstructed monsoon precipitation shows a long-term increasing trend during the last deglaciation and a gradual decrease during the Holocene, with the highest-humidity period occurring in the early Holocene. Our result displays good consistency with the changes in regional mean annual precipitation, summer precipitation, and monsoon intensity during the last deglaciation and the Holocene. On the other hand, the reconstructed mean annual temperature inferred from the *n*-alkane proxy shows a long-term warm trend since the last deglaciation. Our result is consistent with the regional reconstruction of both mean annual and summer temperatures during the last deglaciation, while evident seasonal differences were observed for Holocene records with a cooling trend of summer temperature and a warm trend of mean annual temperature. Comprehensive comparison reveals that monsoon precipitation in the Indian monsoon region is mainly related to changes in the Intertropical Convergence Zone (ITCZ) and land-sea thermal contrast controlled by boreal summer insolation. In addition, the increase in temperature during deglaciation is primarily attributed to the escalation of greenhouse gases (GHGs), while the divergent trend of seasonal temperature during the Holocene is mainly attributed to the changes in local seasonal insolation. Our research emphasizes that monsoon precipitation is a summer signature in the Indian monsoon region, which is consistent with the changes in summer temperature, while contrasting with the changes in mean annual temperature. Therefore, it is necessary to consider the seasonal difference in temperature changes when investigating the hydrothermal combination in Indian monsoon regions.

1. Introduction

The Indian summer monsoon (ISM) is an important component of Asian summer monsoon systems and plays a crucial role in the transfer of heat and moisture from the tropical Indian Ocean to the Asian subcontinent (Sun et al., 2019; Zhang et al., 2017b). The impact of climatic change has significant implications for human activities and economic development, particularly in this densely populated region, where approximately 75% of the world's population is affected (Chen et al., 2014; Xiao et al., 2015). Monsoon climate variability can lead to significant impacts such as widespread droughts or floods, and influence a large population (Yao et al., 2019). Therefore, we investigate the natural fluctuations in precipitation and temperature in the spatial-temporal changes of in the ISM regions to understand the driving factors behind these variations and further enhance our ability to forecast future climate changes.

Numerous studies have been conducted to reconstruct temperature changes during the Holocene using various proxies from geological archives in the ISM region (Wu et al., 2018; Zhao et al., 2021a; Zhang et al., 2017a; Zhang et al., 2023a). However, these reconstructions have yielded complex and sometimes contradictory results in terms of annual and summer temperatures. For instance, mean annual temperature records based on brGDGTs indicate a warming trend (Zhao et al., 2021a; Zhang et al., 2023a), while pollen- and chironomid-based summer temperature records suggest a long-term cooling trend (Wu et al., 2018; Zhang et al., 2017a). Additionally, monsoon hydroclimate variation has also been reconstructed using different climatic archives, such as stalagmite $\delta^{18}O$ (Dykoski et al., 2005; Fleitmann et al., 2003; Liu et al., 2020; Wang et al., 2005), lake carbonate $\delta^{18}O$ (Sun et al., 2019; Wu et al., 2018), and leaf wax δD (Zhao et al., 2021a, 2021b) in southwestern China. These records all indicate a gradual decline in Holocene monsoon precipitation. However, there have been relatively few studies investigating the hydrothermal combination relationship in the Holocene. Sediment records from Tengchongqinghai Lake in southwestern China, for example, show inconsistent changes in warming mean annual temperature and decreased summer monsoon precipitation (Zhao et al.,

2021a). Conversely, a consistent pattern can be observed for the reconstructed summer temperature cooling and summer rainfall decrease in this area (Wu et al., 2018). The characteristics of hydrothermal combinations in the ISM-influenced region since the Holocene remain unclear, which may be due to seasonal bias in temperature and monsoon hydrological changes. Further investigation of the combination pattern of temperature and precipitation in different seasons is necessary.

Isoprenoidal glycerol dibiphytanyl glycerol tetraethers (isoGDGTs) are a suite of membrane lipids produced by some species of archaea, such as Thaumarchaeota and Euryarchaeota (Schouten et al., 2013). The acyclic GDGT-0 is a frequently occurring isoGDGT that can be produced by archaea such as ammonia-oxidizing Thaumarchaeota and anaerobic methane-oxidizing archaea (Blaga et al., 2009; Schouten et al., 2013). IsoGDGTs including 1-3 cyclopentyl moieties (GDGT-1, GDGT-2, GDGT-3) are commonly found in Thaumarchaeota and Crenarchaeota (Schouten et al., 2013). In addition, isoGDGTs also include crenarchaeol, and its isomer crenarchaeol' is produced by Thaumarchaeota (Blage et al., 2011). GDGT-0 and crenarchaeol are much more abundant than GDGTs 1-3 in cultivated Thaumarchaeota (Blage et al., 2011). However, previous studies have suggested that the deep-sea environment rich in methane shows different distribution characteristics of isoGDGT; that is, GDGT-1, GDGT-2 and GDGT-3 are dominant, which is caused by methane-oxidizing archaea with methane hydrates (He et al., 2022; Zhang et al., 2011). These findings indicate that the methane index (GDGT-1+GDGT-2+GDGT-3)/(GDGT-1+GDGT-2+GDGT-3+crenarchaeol+ crenarchaeol′) can serve as a marker for the lipid involvement of methanotrophic archaea (Kim and Zhang et al., 2023; Zhang et al., 2011). Methanotrophic archaea, as anaerobic archaea, contribute more in deep environments, corresponding to higher methane index values, and vice versa (Kim and Zhang et al., 2023; Zhang et al., 2011). Thus, the applicability of the methane index in lake environments has been verified and could reflect changes in water depth and regional precipitation (Cao et al., 2021; Daniels et al., 2021; Yao et al., 2022).

In this study, we present a multiproxy record, including isoGDGTs and *n*-alkanes in lake sediment at Tingming Lake in southwestern China since the last deglaciation. We aimed to: (1) reconstruct effective precipitation and temperature changes simultaneously since the last deglaciation, (2) investigate the regional pattern of hydrothermal combination in different seasons, and (3) elucidate possible causes of monsoon hydroclimate and temperature changes in different seasons.

2. Materials and methods

2.1 Study site

Tingming Lake (26°35′N, 99°01′E, 3,779 m a.s.l.) is located in the Hengduan Mountains, approximately 88.5 km northwest of Liuku County in Yunnan Province, southwestern China (Fig. 1a). This lake has a surface area of 1.5 km^2. The lake basin is surrounded on three sides by mountains. The maximum water depth of Tingming Lake is 19.2 m. Tingming Lake has perennial inflows and outflows, and is mainly recharged by precipitation and lake catchment, and the change in lake water depth is mainly affected by precipitation. The dominant presence in the upper vegetation is made up of sparse Abies forest, which is mostly composed of mixed *Rhododendron* shrubland and herbs (Fig. 1c; Sun et al., 2021; Wang et al., 2023).

This region is influenced by the Indian summer monsoon, which is a subsystem of the Asian summer monsoon circulation. During the summer season, it is mainly affected by warm and moist air currents from the Indian Ocean and the Bay of Bengal, in addition to the impact of the local climate on the Qinghai-Tibet Plateau. Meteorological data from the Liuku station (25°50′N, 98°51′E, 950 m a.s.l.) indicated that the mean annual precipitation (MAP) was 974 mm with 71% rainfall from May to September, and the annual mean temperature was 20.3 ºC over the period of 1977-2017 (Fig. 1b; Sun et al., 2021).

2.2 Sample collection and age model

In fall 2017, a 312 cm-long sediment core (denoted as 17TM3) was drilled from the lake center at a water depth of 16.1 m using a piston corer (Fig. 1c). Modern samples including terrestrial plants, catchment soil, and lake surface sediments, were collected from Tingming Lake and the lake basin. The sediment cores were transported to the laboratory and subsequently subsampled at 1 cm intervals and stored at 4 ^{o}C preserving until analysis.

The dating results of long core 17TM3 were previously reported by Sun et al. (2021) and Wang et al. (2023). AMS ^{14}C dating of 14 terrestrial plant materials and 2 organic sediments or gyttja was used to develop age models for the cores from Tingming Lake. The resulting 16 ^{14}C dates were calibrated to calendar ages and then an age model was reconstructed using the IntCal13 dataset (Reimer et al., 2013). The age model was then developed using a Bayesian model in the Bacon program (Blaauw and Christen, 2011).

2.3 Lipid extraction and GDGT analysis

A total of 146 sediment samples from the long core (17TM3), 7 surface sediment samples, 2 catchment soils and 7 terrestrial plants were analysed for lipid extraction following the below chemical pretreatment (Sun et al., 2021; Yan et al., 2023; Zhang et al., 2022). Freeze-dried samples (3 g) were ultrasonically extracted four times using dichloromethane:methanol (9:1, v/v). After concentrating with N_2, the extracted total lipids were saponified using 6% KOH in methanol solution for 12 hours. The supernatant was collected after adding NaCl and n-hexane and centrifuging. Finally, the neutral supernatant containing *n*-alkanes and GDGTs was extracted through silica gel column chromatography using *n*-alkane and MeOH solutions, respectively.

The *n*-alkanes were measured by an Agilent 7890 Gas Chromatography (GC) device equipped with a flame ionized detector and a split injector, HP1-ms GC column (60 m*0.32 mm, 0.50 μm film thickness) at the State Key Laboratory of Lake Science and Environment in Nanjing Institute of Geography and Limnology. The

detailed oven procedure is to hold for 1 minute at 40 °C, heat to150 °C at a rate10 °C/min, then rise to 310 °C at a rate of 6 °C/min, and finally hold for 60 minutes at 310 °C (Yan et al., 2023; Zhang et al., 2019a).

Multiple *n*-alkane proxies have been proposed to evaluate the lake sediment sources and their relationship with relative climate changes, such as ACL (Ficken et al., 2000; Lin et al., 2023) and total long-chain *n*-alkane concentration ($\sum C_{31\text{-}33}$) (Cranwell et al., 1987),

$$ACL=\sum(n\times C_n)/\sum C_n \ (17\leq n\leq 33)$$

$$\sum C_{31\text{-}33}=\sum C_{31\text{-}33}/\sum C_{16\text{-}33}$$

The GDGTs were analysed using a UPLC-APCI-MS (ACQUITY I-Class plus/Xevo TQ-S system) equipped with two coupled UPLC silica columns (BEH HILIC columns, 3.0*150 mm, 1.7 μm; Waters) in series, fitted with precolumn and maintained at 30 °C. The device can completely separate 5- and 6-methyl isomers by an improved chromatographic procedure. The sample was dissolved in 1000 μl of *n*-hexane and injected with 4 μl. GDGTs were eluted at a constant flow rate of 0.4 ml/min for 80 minutes. The mobile phases of A and B, where A = hexane and B = hexane: isopropanol (9:1, v/v), were run isocratically with 82%A and 18 %B for 25 min, followed by a linear gradient to 65 % A and 35 % B for 25-50 minute, then to 100 % B for 50-60 minute with 20 minute of re-equilibration. GDGTs were ionized in the APCI source at a probe temperature of 550 °C, voltage corona of 5.0 μV, voltage cone of 110 V, gas flow desolvation of 1000 l/h, gas flow cone of 150 l/h and collision gas flow of 0.15 ml/min. GDGT isomers were detected using the selective ion monitoring (SIM) mode to target specific m/z values, including 1302 (GDGT-0), 1300 (GDGT-1), 1298 (GDGT-2), 1296 (GDGT-3) and 1292 (crenarchaeol and crenarchaeol'). The results are expressed as the fraction of the sum of the isoGDGTs based on the integration of the peak areas of the $[M+H]^+$ ions.

The methane index (MI) was calculated according to Zhang et al. (2011) and Kim and Zhang (2023).

MI=(GDGT-1+GDGT-2+GDGT-3)/(GDGT-1+GDGT-2+GDGT-3+crenarchaeol+ crenarchaeol′).

3. Results

Our reconstructed chronology shows that the long core spans the last deglaciation period (16000 years) with an average sedimentation rate of 25 cm/1000 years. The modern *n*-alkane results show clear odd to even predomination among different types of samples (Fig. 2a-2d). In all samples including plants, surface soils, surface sediments and core samples, the *n*-alkane components are in the range from C_{16} to C_{33}, with C_{29} and C_{31} being dominant. The ACL values varied from 27.6 to 29.2 (mean 28.65, Fig. 3a). The C_{31}-C_{33}(%) ranged from 0.38 to 0.30 (mean 0.32, Fig. 3b).

GDGT-0 (42.88% and 43.83%) dominated in isoGDGT in surface sediments and core samples, but crenarchaeol (44.95%) dominated in the surface soils (Fig. 2e). The MI proxy in the core sediments of Tingming Lake showed obvious fluctuations, ranging from 0.12 to 0.62, with an average value of 0.39 (Fig. 3c). The isoGDGT-inferred effective precipitation record displays a long-term increasing trend during the last deglaciation and shows an abrupt drop during the YD period. From the Holocene to the present, humidity records reveal a gradually decreasing trend (Fig. 3c).

4. Discussion

4.1 Climatic significance of multiple proxies in Tingming Lake

GDGTs in lake sediments can originate from lake catchment soils and autochthonous production. Recent studies in Tingming Lake have shown that the contribution of brGDGTs is mainly from authigenic production rather than transportation from catchment soils (Sun et al., 2021). Similarly, the isoGDGTs in Tingming Lake are also from authigenic production rather than exotic input from catchment soils. This is because the distribution of isoGDGTs in core samples is consistent with surface sediments from Tingming Lake but differs from surface soils

in the lake catchment (Fig. 2e). The main source of isoGDGTs in lake sediments is predominantly derived from authigenic production, as supported by many previous studies. For example, the concentration of GDGT-0 in lake sediments is much higher than that in surrounding soils (Blage et al., 2011; Cao et al., 2021; Hu et al., 2016; Inglis et al., 2015; Schouten et al., 2013), indicating an in-situ production of isoGDGTs, which aligns with our results (Fig. 2e). The MI index is widely used to differentiate between anaerobic methane oxidation environments and normal marine conditions (Kim and Zhang, 2021; Zhang et al., 2011). The lower values are likely from the oxidation surface of the sediment in shallow water, whereas the high values reflect anaerobic oxidation of methane in deep-water (Kim and Zhang, 2023; Zhang et al., 2011). As methanogenic archaea thrive in anoxic environments of bottom water or water-sediment interfaces (Blage et al., 2011; Cao et al., 2021). Previous studies have indicated that oxygen concentrations are lower in deeper lake regions, providing a more favourable environment for anaerobic microorganisms (Cao et al., 2021; Daniels et al., 2021; Yao et al., 2022; Zhang et al., 2023b). As a result, the MI index is proposed to reflect variations in lake water depth. For example, there is a positive correlation between MI and lake water depth in Gonghai Lake (Fig. 4; Cao et al., 2021) and Fuxian Lake (Fig. 4; Zheng et al., 2022). Our modern investigation shows a strong positive correlation (R^2=0.57) between the MI index and lake water depth in Tingming Lake (Fig. 4), suggesting that the MI can serve as an indicator of lake water depth changes. Considering that Tingming Lake is a closed, precipitation supply-based lake, the change in lake water depth is affected by precipitation and evaporation, mainly reflecting the change in regional effective precipitation. Therefore, the MI inferred from isoGDGTs can reflect effective precipitation changes in southwestern China.

The ACL records are based on the concentrations of C_{17}~C_{33} alkanes, which represent the average number of carbon atoms (Poynter and Eglinton, 1990). Alkane ACL is a useful indicator of climate change that has previously been found to be related to chain compounds by biosynthesis (Bush et al., 2015; Leider et al., 2013; Zhou et al., 2010). In warmer climates, plants produce longer chain compounds with

higher melting points, while cooler temperate regions produce shorter chain compounds (Bush and McInerney, 2013; Zhou et al., 2010). Consequently, higher ACL values are typically associated with warmer climates, while lower values indicate cooler climates (Leider et al., 2013; Sachse et al., 2006; Wang et al., 2016). The change in the alkane ACL of Tingming Lake may reflect temperature changes, but it is also influenced by other factors, such as precipitation (He et al., 2014; Shi et al., 2021) and plant types (Bush et al., 2013; Nott et al., 2000). In our study, the sediments of Tingming Lake, including surface sediments and core samples (Fig. 2c-2d), are dominated by C_{29}- and C_{31}-alkanes, which account for more than 70% of the total *n*-alkanes. This distribution pattern is consistent with that of surface soil and terrestrial plants (Fig. 2a-2b). Our results align with previous studies on the distribution of *n*-alkanes in the lakes of southwestern China (Yan et al., 2023; Zhao et al., 2021b). Additionally, Tingming Lake has very few aquatic plants and little in-situ production of short chain alkanes. On the other hand, in Yunnan Province, China, precipitation is sufficient, and vegetation growth is mainly controlled by temperature. Thus, the *n*-alkane ACL may be used as an indicator of changes in the mean annual temperature.

4.2 Monsoon hydroclimatic variation in southwestern China

The monsoon precipitation change is reconstructed based on the MI in Tingming Lake since the last deglaciation. Our record reveals a gradual increase in wetness during the last deglaciation with a rapid dry event during the YD period (Fig. 5h). This result is consistent with other palaeoclimatic records in ISM regions, such as rainfall amount and monsoon intensity (Wu et al., 2018; Xu et al., 2019; Zhang et al., 2020, 2023c; Zhao et al., 2021b). For example, the quantitative MAP based on a pollen proxy in Tengchongqinghai Lake demonstrated a continuous increase during the last deglaciation (Fig. 5a; Zhang et al., 2023c), and this result can also be observed from pollen-derived moisture level changes in the same lake (Zhang et al., 2020). The increase in monsoon precipitation is also supported by regional vegetation changes

with an increase in *Pinus* pollen (which flourishes in a semi-humid setting) (Xiao et al., 2015, 2020). In addition, precipitation isotopic records including leaf wax hydrogen isotopes (δD_{wax}) in Lugu Lake (Fig. 5d; Zhao et al., 2021b), carbonate $\delta^{18}O$ in Tiancai Lake (Sun et al., 2019) and stalagmite $\delta^{18}O$ in Dongge Cave (Fig. 5b; Dykoski et al., 2005) in southwestern China exhibit negative excursions, suggesting an intensification of ISM intensity and increasing rainfall. Moreover, a noteworthy millennial-scale oscillation in monsoon precipitation variation was documented during the YD period. This oscillation manifests as a dramatic weakening of the summer monsoon intensity (Fig. 5b; Dykoski et al., 2005; Liu et al., 2020) and a precipitation reduction (Fig. 5a; Zhang et al., 2023c), further leading to a low lake level (Xu et al., 2019). Other multiproxy records, including pollen (Xiao et al., 2020), diatoms (Li et al., 2018) and grain size records (Zhang et al., 2017b), are analysed in lakes sediments. The results from these studies show an increase in drought-resistant plants (Xiao et al., 2020), an increase in coarser grain sizes of mineral particles (Zhang et al., 2017b), and increased water alkalinity (Li et al., 2018), indicating a reduction in regional monsoon precipitation during the YD. In addition, the δD_{wax} record of marine core SO188-342KL in the Bay of Bengal, which carries a signal of rainfall isotopes from terrestrial leaf wax, shows a consistent variation with our effective precipitation records (Fig. 5f; Contreras-Rosales et al., 2014). From the same region, sea surface salinity records derived from $\delta^{18}O_{sw}$ in cores RC12-344 and KL126 (Fig. 5g; Kudrass et al., 2001; Rashid et al., 2007), which are influenced by monsoon rainfall in the Asian subcontinent through Irrawaddy River drainage (Zhang et al., 2017b), show consistent long-term trends and millennial-scale variations with our results. Therefore, monsoon precipitation shows a gradual increasing trend in the ISM region, superimposed by a pronounced millennial-scale dry event during the YD period.

During the Holocene period, reconstructed effective precipitation presents a gradual decreasing trend, with the highest value in the early Holocene (Fig. 5h). Consistent changes can also be documented by other geological archives, including lakes (Li et al., 2018; Hou et al., 2021; Rades et al., 2015; Wu et al., 2018; Xiao et al.,

2020; Zhang et al., 2023c; Zhao et al., 2021a, 2021b) and stalagmites (Dykoski et al., 2005; Fleitmann et al., 2003; Liu et al., 2020; Wang et al., 2005). For example, the MAP record, reconstructed by high-resolution pollen from Tengchongqinghai Lake and Caohai Lake in southwestern China (Fig. 5a; Zhang et al., 2023c), shows a gradual moisture reduction trend from the early to late Holocene. This can also be supported by changes in elevated lake levels, indicating wetter conditions during the early Holocene (Hou et al., 2021; Rades et al., 2015). Additionally, the gradual shift to wettest environment in the early Holocene is also supported by pollen (Xiao et al., 2020), diatoms (Li et al., 2018), and grain size (Zhang et al., 2017b) in lake sediment records, in which the increased semi-humid evergreen broad-leaved forest, increased water acid and increased small grain-size fraction resulted from increased monsoonal precipitation. Similarly, the highest monsoon rainfall is related to an enhanced ISM in the early Holocene, as indicated by precipitation isotopic records from stalagmites in southern Oman (Fig. 5c, Qunf Cave, Fleitmann et al., 2003) and southwestern China (Fig. 5b; Dykoski et al., 2005; Liu et al., 2020; Wang et al., 2005), and from lacustrine δD_{wax} records (Fig. 5d; Zhao et al., 2021a, 2021b) and carbonate $\delta^{18}O$ record (Fig. 5e; Wu et al., 2018) in southwestern China, all consistently demonstrating a negative trend. In addition, it is worth noting that the MAP record shows a declining tendency throughout the entire Holocene and is consistent with records of monsoon intensity and monsoon rainfall (Fig. 7a-7e, 7h). This is because precipitation in southwestern China predominantly occurs during the summer season, with approximately 70% of the rainfall falling between June and August. In addition, marine records from the Bay of Bengal suggest a gradual decrease in rainfall throughout the Holocene. This is indicated by increased δD_{wax} values (Fig. 5f; site SO188-342KL; Contreras-Rosales et al., 2014) and rising sea surface salinity (Fig. 5g; site RC12-344 and KL126; Kudrass et al., 2001; Rashid et al., 2007). Furthermore, this pattern aligns with records in and around the Arabian Seas, which display higher rainfall and stronger monsoon activity in the early Holocene than in the late Holocene (Anand et al., 2008; Jung et al., 2002). In summary, our study of Tingming Lake presents a continuous decreasing trend in precipitation variations in the Holocene.

4.3 Seasonal temperature variation in southwestern China

Our reconstructed temperature change inferred from *n*-alkane ACL displays a long-term warming trend since the last deglaciation in Tingming Lake (Fig. 6b). To investigate the temperature change, we compiled quantitative temperature records during the last deglaciation and the Holocene. During the last deglaciation, our reconstructed record aligns with numerous regional temperature records, showing a continuous warming trend (Fig. 6). For example, the brGDGT-derived mean annual temperature at Tengchongqinghai Lake (Fig. 6c; Zhao et al., 2021a), Chenghai Lake (Sun et al., 2023), XimenCo Lake (Herzschuh et al., 2014), and Hongyuan peat (Yan et al., 2021) in southwestern China, displays a gradual warming trend. Likewise, the diatom- and chironomid-derived summer temperatures reveal a gradual slight warming trend at Tiancai Lake (Fig. 6f; Wang et al., 2023; Zhang et al., 2019b), as does the alkenone-based temperature at Qinghai Lake (Fig. 6g; Hou et al., 2016) and the pollen-based temperature at Xingyun Lake (Wu et al., 2018). Meanwhile, integrated seasonal temperature records, including mean annual temperature (Fig. 6a) and summer temperature (Fig. 6e), suggest a continuing warming trend in the last deglaciation (Zhang et al., 2022). In addition, sudden temperature drops during the YD period are identified in our reconstructed result (Fig. 6b) and regional mean annual temperature records (Fig. 6a, 6c-6d), which interrupt the overall warming trend of the last deglaciation. However, compared to the mean annual temperature records (Fig. 6a-6d), the YD signature is less pronounced in summer temperature records, such as the chironomid-inferred (Fig. 6f; Zhang et al., 2019b), alkenone-based (Fig. 6g; Hou et al., 2016) and diatom-inferred records (Wang et al., 2023). Therefore, the reconstructed temperature records in southwestern China indicate an overall warming trend during the last deglaciation, whereas the millennial-scale YD cold event is not evident in the summer temperature records.

During the Holocene, reconstructed temperature records indicate distinct seasonal variations in southwestern China, which is inferred from our results and reviewed temperature data (Fig. 6). For example, the brGDGT-based mean annual

temperature record indicates a well-defined gradual warming trend at Lugu Lake (Fig. 6d; Zhao et al., 2021a), Tengchongqinghai Lake (Fig. 6c; Zhao et al., 2021a), Chenghai Lake (Zhang et al., 2023c) and Hongyuan peat (Yan et al., 2021). Additionally, the integrated mean annual temperature records throughout the Holocene confirmed this overall warming trend (Fig. 6a; Zhang et al., 2022). However, the temperature trends in other seasons are different. Summer temperature records show a long-term cooling pattern, as observed in the chironomid-inferred temperature record from Tiancai Lake (Fig. 6f; Zhang et al., 2017a), the alkenone-reconstructed temperature record from Qinghai Lake (Fig. 6g; Hou et al., 2019), and the pollen-inferred temperature records from Xingyun Lake (Wu et al., 2018). Similarly, the recently stacked entire Holocene summer temperature record suggests a general cooling trend towards the present in southwestern China (Fig. 6e; Chen et al., 2020; Zhang et al., 2022). In addition, it is worth noting that our temperature record also displays a distinct decline-temperature period at 3000-4500 years. A similar trend can be observed for the diatom-inferred mean annual temperature in same lake (Wang et al., 2023), which is similar to the mean annual temperature records in Tengchongqinghai Lake and Lugu Lake (Fig. 6c-6d; Zhao et al., 2021a), and the summer temperature record in Qinghai Lake (Fig. 6g; Hou et al., 2016). Previous studies have suggested that the temperature cooling between 3000-4500 years may be related to a southwards migration of the Intertropical Convergence Zone (ITCZ) (Hou et al., 2016), which is in line with our reconstructed result (Fig. 7a, 7f). In summary, the reconstructed Holocene temperature records show distinct seasonal biases in southwestern China with a long-term warming trend for mean annual temperature but a gradually cooling trend for summer temperature.

4.4 Hydrothermal combination in southwestern China and its driving mechanism

We further investigated the hydrothermal combination and its potential driving mechanism since deglaciation in southwestern China. During the last deglaciation, the monsoon hydrological and temperature records show consistent changes towards a

gradually warm-wet trend (Fig. 7a-7d). Despite changes in the amplitude of seasonal temperature, the overall pattern of summer and mean annual temperature is consistent in the last deglaciation (Fig. 7a-7b). Similarly, the trends of monsoon precipitation and mean annual temperature are also consistent (Fig. 7a, 7c). By comparison, the observed temperature changes align with the global warming trend identified by proxy-based palaeotemperature reconstructions and climate model simulations (Fig. 7a-7b; Shakun et al., 2012; Liu et al., 2014). Proxy-based temperature warming tendencies are attributed to increasing CO_2 concentrations in the last deglaciation (Shakun et al., 2012; Zhang et al., 2022). Similarly, the simulated results of the CCSM3 model indicate that the main driver of deglaciation warming is the rise in atmospheric greenhouse gases (Zhang et al., 2022). Thus, the increased temperature is primarily attributed to the rising CO_2 concentration during deglaciation (Fig. 7g; Lüthi et al., 2008). In addition, reconstructed monsoon hydrological records show good consistency with the ITCZ variations in both the long-term trend and millennial-scale fluctuations (Fig. 7c-7d). Previous studies have indicated that the ITCZ could influence rainfall changes in southwestern China (Deplazes et al., 2013; Dykoski et al., 2005; Fleitmann et al., 2023; Sun et al., 2019). During the last deglaciation, the northwards displacement of the ITCZ (Fig. 7f; Haug et al., 2002) followed by the gradual increase in boreal summer insolation (Fig. 7h; Laskar et al., 2004), can strengthen the ISM intensity and then increase rainfall (Fig. 7c-7d; Dykoski et al., 2005; Zhang et al., 2023c; Zhao et al., 2021b). Meanwhile, the ISM intensity is influenced by the thermal contrast between the Indian Ocean and the Asian land mass (Fig. 7e; Böll et al., 2015; Naidu et al., 2005). This temperature difference leads to the transport of water vapour to the Asian subcontinent, which in turn affects monsoon rainfall (Fig. 7c-7d; Dykoski et al., 2005; Zhang et al., 2023c; Zhao et al., 2021b). Additionally, proxy-derived hydrothermal combination indicates significant cooling and drying climatic conditions at the millennial time scale during the YD period (Fig. 7a, 7c-7d), which are probably related to the Atlantic Meridional Overturning Circulation (AMOC, McManus et al., 2004). Previous studies have suggested a relatively strong correlation between temperature records and the strength of AMOC

(Sun et al., 2021; Wu et al., 2019; Zhang et al., 2022) inferred from Pa/Th (McManus et al., 2004). Specifically, the YD event occurred during the long-term warming phase due to the influx of freshwater into the North Atlantic, causing the shutdown of the AMOC (McManus et al., 2004). This disruption reduced heat and moisture transfer from low latitudes to the middle and high latitudes (Shakun et al., 2012). Additionally, the weakened AMOC could further result in the southwards displacement of the ITCZ and the weakening of the monsoon intensity and rainfall (Fig. 7c-7d; Dykoski et al., 2005; Zhang et al., 2023c; Zhao et al., 2021b).

Due to the obvious seasonal bias in Holocene temperature, seasonal differences need to be considered to understand the Holocene hydrothermal combination in southwest China. At the annual scale, the hydrothermal combination exhibits opposite variations, manifesting as a warming trend in temperature (Fig. 7a) and a decline in MAP (Fig. 7c). In contrast, at the summer scale, the hydrothermal combination displays a consistent shift from a warm and humid climate in the early Holocene to gradually becoming cold and dry conditions. In southwestern China, the reconstructed annual mean temperature records align with the simulated result of regional temperature with a long-term warming trend (Zhang et al., 2022), consistent with the increase in local annual insolation (Fig. 7h; Laskar et al., 2004). However, the continuous decrease in proxy-reconstructed summer temperature records coherent with the regional simulated summer temperature records (Fig. 7b; Marcott et al., 2013), is in accord with the decrease in local summer insolation (Fig. 7h; Laskar et al., 2004). In the long-term trend, the monsoon hydrological records in southwestern China are notably consistent with summer insolation (Fleitmann et al., 2003; Liu et al., 2020; Wang et al., 2005; Wu et al., 2018). The decreasing summer insolation weakens the monsoon intensity and further reduces the monsoon precipitation in our study area (Fig. 7c-7d, 7h; Dykoski et al., 2005; Zhang et al., 2023c; Zhao et al., 2021b). Moreover, the persistent decline in monsoon precipitation may be related to the southwards migration of the ITCZ (Fig. 7f; Fleitmann et al. 2003; Haug et al., 2001) and the decreasing thermal contrast between the Indian Ocean and Asian subcontinent (Fig. 7e; Böll et al., 2015; Naidu et al., 2005), which results in a decrease in

meridional water vapour transport from tropical regions to the Asian subcontinent (Sun et al., 2019; Zhang et al., 2017b).

In summary, the monsoon variation is a summer phenomenon, reflecting summer conditions, rather than an annual condition. Seasonal changes in temperature need to be considered when investigating the hydrothermal combination in the southwestern China region in the future.

5. Conclusions

In this study, we investigated the changes in hydrothermal combinations by multiple proxies, including isoGDGTs and *n*-alkanes from Tingming Lake. Our main results are as follows:

(1) Modern investigation indicates that isoGDGTs are primarily produced in situ, as inferred from the different distribution pattern between catchment soils and lake sediments. The MI calculated from isoGDGTs can effectively reflect the changes in lake water depth and further indicate the variation in regional effective precipitation. High MI values indicate high effective precipitation, and vice versa. *n*-Alkanes in Tingming Lake sediments are dominated by long-chain C_{29} and C_{31}, mainly from catchment plants. The ACL index calculated from *n*-alkanes is mainly controlled by regional temperature, which can reflect the changes in regional mean annual temperature.

(2) Our reconstructed mean annual temperature displays a long-term warming trend during the last deglaciation and Holocene. Through further comparison, both summer and mean annual temperature show a warming trend during the last deglaciation, while Holocene summer temperature shows a cooling trend but a warming trend for mean annual temperature. Our reconstructed monsoon precipitation exhibits significant consistency with the changes in regional MAP, summer precipitation, and monsoon intensity during the last deglaciation and the Holocene.

(3) By regional comparison, the hydrothermal combination shows a consistent

increase change during the last deglaciation in southwestern China. In the Holocene, the hydrothermal combination exhibits declining pattern in the summer season but is inconsistent annually. The monsoon rainfall is attributed to NH summer insolation through modulating the meridional migration of the ITCZ and thermal difference between the land and oceans, while the warming temperature is primarily influenced by rising CO_2 during the last deglaciation, and the summer and mean annual temperature in the Holocene are driven by local summer and annual insolation, respectively.

Declaration of Competing Interest

The authors declare that they have no known competing financial interests.

Acknowledgments

We thank Cheng Zhao, Xiangdong Yang, Qi Lin, Zhenyu Ni for field assistance. This work was supported by the National Natural Science Foundation of China (42371167), the Strategic Priority Research Program of Chinese Academy of Sciences (XDB40000000), Shandong Provincial Natural Science Foundation (ZR2022QD131), State Key Laboratory of Loess and Quaternary Geology, Institute of Earth Environment, CAS (SKLLOG2226).

References

Anand, P., Kroom, D., Singh, A.D., et al. 2008. Coupled sea surface temperature-seawater $\delta^{18}O$ reconstructions in the Arabian Sea at the millennial scale for the last 35 ka. Paleoceanography 23 (4), PA4207. https://doi/10.1029/2007PA001564.

Blaauw, M., Christen, J. A. 2011. Flexible paleoclimate age-depth models using an

autoregressive gamma process. Bayesian Analysis, 6(3), 457-474. https://doi.org/10.1214/11-BA618. https://doi/10.1214/11-BA618.

Blaga, C.I., Reichart, G.-J., Heiri, O., et al. 2009. Tetraether membrane lipid distributions in water column particulate matter and sediments: a study of 47 European lakes along a north–south transect. J. Paleolimnol. 41, 523-540. https://doi.org/10.1007/s10933-008-9242-2.

Blaga, C.I., Reichart, G.-J., Vissers, E.W., et al. 2011. Seasonal changes in glycerol dialkyl glycerol tetraether concentrations and fluxes in a perialpine lake: implications for the use of the TEX 86 and BIT proxies. Geochimica et Cosmochimica Acta 75: 6416-6428. https://doi.org/10.1016/j.gca.2011.08.016.

Böll, A., Schulz, H., Munz, P., et al. 2015. Contrasting sea surface temperature of summer and winter monsoon variability in the northern Arabian Sea over the last 25 ka. Palaeogeogr Palaeoclimatol Palaeoecol, 426:10-21. https://doi.org/10.1016/j.palaeo.2015.02.036.

Bush, R.T., McInerney, F.A. 2013. Leaf wax n-alkane distributions in and across modern plants: implications for paleoecology and chemotaxonomy. Geochim Cosmochim Acta, 117(15):161-179. https://doi.org/10.1016/j.gca.2013.04.016.

Cao, J.T., Rao, Z.G., Shi, F.X., et al. 2021. Lake-level records support a mid-Holocene maximum precipitation in northern China. Science China Earth Sciences, 64. https://doi.org/10.1007//s11430-020-9833-3.

Chen, F.H., Zhang, J.F., Liu, J.B., et al. 2020. Climate change, vegetation history, and landscape responses on the Tibetan Plateau during the Holocene: A comprehensive review. Quaternary Science Reviews, 243, 106444. https://doi.org/10.1016/j.quascirev.2020.106444.

Chen, F.H., Chen, X.M., Chen, J.H., et al. 2014. Holocene vegetation history, precipitation changes and Indian summer monsoon evolution documented from sediments of Xingyun Lake, southwest China. J. Quat. Sci. 29 (7), 661e674. https://doi.org/10.1002/jqs.2735.

Contreras-Rosales, L.A., Jennerjahn, T., Tharammal, T., et al. 2014. Evolution of the Indian Summer Monsoon and terrestrial vegetation in the Bengal region during

the past 18 ka. Quaternary Science Reviews, 102, 133-148. https://doi.org/10.1016/j.quascirev.2014.08.010.

Cranwell, P.A., Eglinton, G., Robinson, N. 1987. Lipids of aquatic organisms as potential contributors to lacustrine sediments. Org. Geochem. 11, 513-527. https://doi.org/10.1016/0146-6380(84)90035-4.

Daniels, W.C., Castaneda, I.S., Salacup, J.M., et al. 2021. Archaeal lipids reveal climate-driven changes in microbial ecology at Lake El'gygytgyn (Far East Russia) during the Plio-Pleistocene. Journal of Quaternary Science, 00(0)1-15. https://doi.org/10.1002/jqs.3347.

Deplazes, G., Lückge, A., Peterson, L.C., et al. 2013. Links between tropical rainfall and North Atlantic climate during the last glacial period. Nat. Geosci, 6 (3), 213e217. https://doi.org/10.1038/NGEO1712

Dykoski, C. A., Edwards, R. L., Cheng, H., et al. 2005. A high-resolution, absolute-dated Holocene and deglacial Asian monsoon record from Dongge Cave, China. Earth and Planetary Science Letters, 233, 71-86. https://doi.org/10.1016/j.epsl.2005.01.036

Ficken, K.J., Li, B., Swain, D.L., et al. 2000. An n-alkane proxy for the sedimentary inputs of submerged/floating freshwater aquatic macrophytes. Org. Geochem, 31, 745-749. https://doi.org/10.1016/S0146-6380(00)00081-4.

Fleitmann, D., Burns, S.J., Mudelsee, M., et al. 2003. Holocene forcing of the Indian monsoon recorded in a stalagmite from southern Oman. Science, 300(5626), 1737-1739. https://doi.org/10.1126/science.1083130.

Haug, G. H., Hughen, K. A., Sigman, D. M., et al. 2001. Southward migration of the intertropical convergence zone through the Holocene. Science, 293, 1304-1308. https://doi.org/10.1126/science.1059725

He, J., Jia, J.Y. Guo, W., et al. 2022. Archaeal tetraether lipids and their biphytane carbon isotope composition in sediments along an estuarine biogeochemical gradient. Geochimica et Cosmochimica Acta, 318, 452-467. https://doi.org/10.1016/j.gca.2021.12.015.

He, Y., Zheng, Y., Pan, A., et al. 2014. Biomarker-based reconstructions of Holocene

Lake-level changes at Lake Gahai on the northeastern Tibetan Plateau. The Holocene, 24, 405-412. https://doi.org/10.1177/0959683613519689.

Herzschuh, U., Borkowski, J., Schewe, J., et al. 2014. Moisture-advection feedback supports strong early-to-mid Holocene monsoon climate on the eastern Tibetan Plateau as inferred from a pollen-based reconstruction. Palaeogeogr. Palaeoclimatol. Palaeoecol, 402, 44-54. https://doi.org/10.1016/j.palaeo.2014.02.022.

Hou, J.Z., Huang, Y.S., Zhao, J.T., et al. 2016. Large Holocene summer temperature oscillations and impact on the peopling of the northeastern Tibetan Plateau. Geophysical research letters, 43, 1323-1330. https://doi.org/10.1002/2015gl067317.

Hou, Y.D., Long, H., Shen, J., et al. 2021. Holocene lake-level fluctuations of Selin Co on the central Tibetan plateau: Regulated by monsoonal precipitation or meltwater? Quaternary Science Reviews, 261, 106919. https://doi.org/10.1016/j.quascirev.2021.106919.

Hu, J.F., Zhou, H.D., Peng, P.A., et al. 2016. Seasonal variability in concentrations and fluxes of glycerol dialkyl glycerol tetraethers in Huguangyan Maar Lake, SE China: Implications for the applicability of the MBT–CBT paleotemperature proxy in lacustrine settings. Chemical Geology, 420, 200–212. http://dx.doi.org/10.1016/j.chemgeo.2015.11.008.

Inglis, G. N., Farnsworth, A., Lunt, D. et al. 2015. Descent toward the Icehouse: Eocene sea surface cooling inferred from GDGT distributions, Paleoceanography, 29, http://dx.doi.org/10.1002/2014PA002723.

Jung, S.J.A., Davies, G.R., Ganssen, G., et al. 2002. Decadal-centennial scale monsoon variations in the Arabian Sea during the Early Holocene. Geochemistry Geophysics Geosystems, (10). https://doi.org/10.1029/2002GC000348.

Kim, B., Zhang, Y.G. 2023. Methane Index: Towards a quantitative archaeal lipid biomarker proxy for reconstructing marine sedimentary methane fluxes Geochimica et Cosmochimica Acta, 354, 74-87. https://doi.org/10.1016/j.gca.2023.06.008.

Kudrass, H.R., Hofmann, A., Doose, H., et al. 2001. Modulation and amplification of climatic changes in the Northern hemisphere by the Indian summer monsoon during the past 80 k.y. Geology, 29 (1), 63-66. https://doi.org/10.1130/0091-7613(2001)029<0063:MAAOCC>2.0.CO;2.

Laskar, J., Robutel, P., Joutel, F., et al. 2004. A long term numerical solution for the insolation quantities of the Earth. Astronomy & Astrophysics, 428, 261–285. https://doi.org/10.1051/0004-6361:20041335.

Leider, A., Hinrichs, K.-U, Schefuß, E., et al. 2013. Distribution and stable isotopes of plant wax derived n-alkanes in lacustrine, fluvial and marine surface sediments along an Eastern Italian transect and their potential to reconstruct the hydrological cycle. Geochim Cosmochim Acta, 117:16-32. http://dx.doi.org/10.1016/j.gca.2013.04.018.

Li, Y.L., Chen, X., Xiao, X.Y., et al. 2018. Diatombased inference of Asian monsoon precipitation from a volcanic lake in southwest China for the last 18.5 ka. Quat. Sci. Rev, 182, 109e120. https://doi.org/10.1016/j.quascirev.2017.11.021.

Lin, D.R., Zhong, W., Lin, Y.B., et al. 2023. Organic matter source traced by n-alkane records derived from lacustrine sediments from Daping swamp in the western Nanling Mountains (South China) and its response to climatic variability since the last deglacial. Palaeogeography, Palaeoclimatology, Palaeoecology, 605, 111217. https://doi.org/10.1016/j.palaeo.2022.111217.

Liu, G.X., Li, X., Chiang, H.W., et al. 2020. On the glacial-interglacial variability of the Asian monsoon in speleothem $\delta^{18}O$ records. Science Advances, 6(7), 1-10. https://doi.org/10.1126/sciadv.aay8189

Liu, Z.Y., Zhu, J., Rosenthal, Y., et al. 2014. The Holocene temperature conundrum. Proceedings of the National Academy of Sciences, 111, E3501-E3505. https://doi.org/10.1073/pnas.1407229111.

Lüthi, D., Le Floch, M. L., Bereiter, B., et al. 2008. High-resolution carbon dioxide concentration record 650,000-800,000 years before present. Nature, 453, 379–382. https://doi.org/10.1038/nature06949.

Marcott, S.A., Shakun, J.D., Clark, P. U., et al. 2013. A Reconstruction of Regional

and Global Temperature for the Past 11,300 Years. Science 339, 1198-1201. https://doi.org/10.1126/science.1228026.

McManus, J.F., Francois, R., Gherardi, J.M., et al. 2004. Collapse and rapid resumption of Atlantic meridional circulation linked to deglacial climate changes. Nature 428, 834-837. https://doi.org/10.1038/nature02494.

Naidu, P.D., Malmgren, B.A., 2005. Seasonal sea surface temperature contrast between the Holocene and last glacial period in the western Arabian Sea (Ocean Drilling Project Site 723A): modulated by monsoon upwelling. Paleoceanography 20. http://dx.doi.org/10.1029/2004PA001078

Nott, C.J., Xie, S.C., Avsejs, L.A., et al. 2000. n-Alkane distributions in ombrotrophic mires as indicators of vegetation change related to climatic variation. Organic Geochemistry 31, 231-235. https://doi.org/10.1016/S0146-6380(99)00153-9.

Poynter, J., Eglinton, G., 1990. Molecular composition of three sediments from Hole 717C: the Bengal Fan. Proc. Ocean Drill. Prog. Sci. Res. 116, 155–161. https://doi.org/10.2973/odp.proc.sr.116.151.1990.

Rades, E.F., Tsukamoto, S., Frechen, M., et al. 2015. A lake-level chronology based on feldspar luminescence dating of beach ridges at Tangra Yum Co (southern Tibet). Quat. Res. 83 (3), 469e478. http://dx.doi.org/10.1016/j.yqres.2015.03.002.

Rashid, H., Flower, B. P., Poore, R. Z., et al. 2007. A ~25ka Indian Ocean monsoon variability record from the Andaman Sea. Quaternary Science Reviews, 26(19-21), 2586-2597. https://doi.org/10.1016/j.quascirev.2007.07.002.

Reimer, P. J., Bard, E., Bayliss, A., et al. 2013. IntCal13 and Marine13 radiocarbon age calibration curves 0-50,000 yr cal. Radiocarbon, 55(4), 1869-1887. https://doi.org/10.2458/azu_js_rc.55.16947.

Sachse, D., Radke, J., Gleixner, G. 2006. δD values of individual n-alkanes from terrestrial plants along a climatic gradient–Implications for the sedimentary biomarker record. Org Geochem.; 37(4):469-483. https://doi.org/10.1016/j.orggeochem.2005.12.003.

Schouten, S., Hopmans, E.C., Sinninghe Damsté, J.S. 2013. The organic geochemistry

of glycerol dialkyl glycerol tetraether lipids: A review. Organic Geochemistry, 54, 19-61. https://doi.org/10.1016/j.orggeochem.2012.09.006

Shakun, J.D., Clark, P.U., He, F., et al. 2012. Global warming preceded by increasing carbon dioxide concentrations during the last deglaciation. Nature 484, 49–54. https://doi.org/10.1038/nature10915.

Shi, M.R., Han, J.M., Wang, G.A., et al. 2021. A long-term investigation of the variation in leaf wax n-alkanes responding to climate on Dongling Mountain, north China. Quaternary International, 592, 67-79. https://doi.org/10.1016/j.quaint.2021.04.020

Sun, W.W., Zhang, E.L., Jiang, Q.F., et al. 2023. Temperature changes during the last deglaciation and early Holocene in southwest China. Global and Planetary Change, 229, 104238. https://doi.org/10.1016/j.gloplacha.2023.104238

Sun, W.W., Zhang, E.L., Shulmeister, J., et al. 2019. Abrupt changes in indian summer monsoon strength during the last deglaciation and early Holocene based on stable isotope evidence from Lake Chenghai, Southwest China. Quat. Sci. Rev. 218, 1-9. https://doi.org/10.1016/j.quascirev.2019.06.006.

Sun, X.S., Zhao, C., Zhang, C., et al. 2021. Seasonality in Holocene temperature reconstructions in Southwestern China. Paleoceanogr. Paleoclimatol. 36. https://doi.org/10.1029/2020PA004025e2020PA004025.

Wang, Q., Yang, X.D., Song, B. 2023. Patterns of last-deglacial diatom-inferred summer temperature variability and ecological thresholds in the alpine lakes from southeastern margin of the Tibetan Plateau, Global and Planetary Change 229, 104235. https://doi.org/10.1016/j.gloplacha.2023.104235

Wang, X., Huang, X., Sachse, D., et al. 2016. Molecular Paleoclimate Reconstructions over the last 9 ka from a Peat Sequence in South China. PLoS ONE, 11, e0160934. https://doi.org/10.1371/journal.pone.0160934.

Wang, Y.J., Cheng, H., Edwards, R.L., et al. 2005. The Holocene Asian monsoon: links to solar changes and North Atlantic climate. Science, 308, 5723, 854-857. https://doi.org/10.1126/science.1106296.

Wu, D., Chen, X.M., Lv, F.Y., et al. 2018. Decoupled early Holocene summer

temperature and monsoon precipitation in southwest China. Quaternary Science Reviews, 193, 54-67. https://doi.org/10.1016/j.quascirev.2018.05.038.

Xiao, X.Y., Shen, J., Haberle, S.G., et al., 2015. Vegetation, fire, and climate history during the last 18500 cal a BP in South-Western Yunnan Province, China. J. Quat. Sci. 30 (8), 859-869. https://doi.org/10.1002/jqs.2824.

Xiao, X.Y., Yao, A., Hillman, A.L., et al. 2020. Vegetation, climate and human impact since 20 ka in Central Yunnan Province based on high-resolution pollen and charcoal records from Dianchi, southwestern China. Quat. Sci. Rev. 236, 106297. https://doi.org/10.1016/j.quascirev.2020.106297.

Xu, H., Goldsmith, Y., Lan, J.H., et al. 2020. Juxtaposition of western Pacific subtropical high on Asian Summer Monsoon shapes subtropical East Asian precipitation. Geophysical Research Letters, 47, e2019GL084705. https://doi.org/10.1029/2019GL084705.

Yan, T.L., Zhang, C., Zhang, H.X., et al. 2023. Quantitative temperature and relative humidity changes recorded by the Lake Cuoqia in the southeastern Tibetan Plateau during the past 300 years. Frontiers in Ecology and Evolution, 11:1119869. https://doi.org/10.3389/fevo.2023.1119869.

Yao, T.D., Xue, Y., Chen, D., et al. 2019. Recent third pole's rapid warming accompanies cryospheric melt and water cycle intensification and interactions between monsoon and environment: Multidisciplinary approach with observations, modeling, and analysis. Bulletin of the American Meteorological Society, 100(3), 423-444. https://doi.org/10.1175/BAMS-D-17-0057.1

Yan, T.L., Zhang, C., Zhang, H.X., et al. 2023. Quantitative temperature and relative humidity changes recorded by the Lake Cuoqia in the southeastern Tibetan Plateau during the past 300 years. Front. Ecol. Evol. 11:1119869. https://doi: 10.3389/fevo.2023.1119869

Yan, T.L., Zhao, C., Yan, H., et al. 2021. Elevational differences in Holocene thermal maximum revealed by quantitative temperature reconstructions at ~30◦ N on eastern Tibetan Plateau. Palaeogeogr. Palaeoclimatol. Palaeoecol. 570, 110364. https://doi.org/10.1016/j.palaeo.2021.110364.

Yao, Y., Huang, Y.S., Zhao, J.J., et al. 2022. Lipid biomarkers in Lake Wudalianchi record abrupt environmental changes from the volcanic eruption in 1776. Organic Geochemistry, 164, 104349. https://doi.org/10.1016/j.orggeochem.2021.104349.

Zhang, C., Zhao C., Yu, S.Y., et al. 2023a. Divergent trends of changes in annual mean and summer temperature in southwestern China during the Holocene, Global and Planetary Change. https://doi.org/10.1016/j.gloplacha.2023.104218.

Zhang, C., Zhao, C., Yu, S., et al. 2022. Seasonal imprint of Holocene temperature reconstruction on the Tibetan Plateau. Earth-Science Reviews, 226, 103927. https://doi.org/10.1016/j.earscirev.2022.103927.

Zhang, C., Zhao, C., Zhou, A.F., et al. 2019a. Late Holocene lacustrine environmental and ecological changes caused by anthropogenic activities in the Chinese Loess Plateau. Quaternary Science Reviews 203, 266e277. https://doi.org/10.1016/j.quascirev.2018.11.020

Zhang, E.L., Chang, J., Cao, Y.M., et al. 2017a. Holocene high-resolution quantitative summer temperature reconstruction based on subfossil chironomids from the southeast margin of the Qinghai-Tibetan Plateau. Quaternary Science Reviews, 165, 1-12. https://doi.org/10.1016/j.quascirev.2017.04.008.

Zhang, E.L., Zhao, C., Xue, B., et al. 2017b. Millennial-scale hydroclimate variations in southwest China linked to tropical Indian Ocean since the Last Glacial Maximum. Geology 45, 435e438

Zhang, E.L., Chang, J., Shulmeister, J., et al. 2019b. Summer temperature fluctuations in Southwestern China during the end of the LGM and the last deglaciation. Earth Planet. Sci. Lett. 509, 78-87. https://doi.org/10.1016/j.epsl.2018.12.024.

Zhang, T., Wang, G., Wang, Y.L., et al. 2023b. Long-term drying trends since the mid-Holocene in the Qaidam Basin. Catena 228, 107145. https://doi.org/10.1016/j.catena.2023.107145.

Zhang, X., Zheng, Z., Huang, K., et al. 2023c. Quantification of Asian monsoon variability from 68 ka BP through pollen-based climate reconstruction. Science Bulletin, 68, 713-722. https://doi.org/10.1016/j.scib.2023.03.013.

Zhang, X., Zheng, Z., Huang, K.Y., et al. 2020. Sensitivity of altitudinal vegetation in southwest China to changes in the Indian summer monsoon during the past 68000 years. Quaternary Science Reviews, 239: 106359. https://doi.org/10.1016/j.quascirev.2020.106359.

Zhang, Y.G., Zhang, C.L., Liu, X.L., et al. 2011. Methane Index: A tetraether archaeal lipid biomarker indicator for detecting the instability of marine gas hydrates. Earth and Planetary Science Letters 307, 525-534.

Zhao, C., Rohling, E.J., Liu, Z., et al. 2021a. Possible obliquity-forced warmth in southern Asia during the last glacial stage. Science Bulletin, 66, 1136-1145. https://doi.org/10.1016/j.scib.2020.11.016.

Zhao, C., Cheng, J., Wang, J., et al. 2021b. Paleoclimate Significance of Reconstructed Rainfall Isotope Changes in Asian Monsoon Region. Geophysical Research Letters, 48, e2021GL092460. https://doi.org/10.1029/2021GL092460.

Zheng, P.B., Yang, H., Pancost, R.D., et al. 2022. Dissolved oxygen concentrations influence the distribution of isoGDGTs in a deep Lake Fuxian in China: Implications for the use of TEX_{86} in stratified lakes, Organic Geochemistry, 173, 104485. https://doi.org/10.1016/j.orggeochem.2022.104485.

Zhou, W.J., Zheng, Y.H., Meyers, P.A., et al. 2010. Postglacial climate-change record in biomarker lipid compositions of the Hani peat sequence, Northeastern China. Earth Planet. Sci. Lett. 294, 37-46. https://doi.org/10.1016/j.epsl.2010.02.035.

Figure. 1 Location and setting. (a) Map showing the location of our study site (Tingming Lake, red square) and other referenced sites in this text (green dots). Lugu Lake (LG; Zhao et al., 2021a, 2021b), Tengchongqinghai Lake (TCQH; Zhang et al., 2023c; Zhao et al., 2021a), Caohai Lake (CH; Zhang et al., 2023c), Xingyun Lake (XY; Wu et al., 2018), Dongge Cave (DG; Dykoski et al., 2005; Wang et al., 2005), Qunf Cave (QF; Fleitman et al., 2003), SO188-342KL (Contreras Rosales et al., 2014), RC12-344 (Rashid et al., 2007), SO90-93KL (Böll et al., 2015), and ODP723A (Naidu et al., 2005); (b) Mean monthly temperature and precipitation at the Liuku Meteorological Station, Yunnan Province, China (data retrieved from the Meteorological Administration of China, http://data.cma.cn/); (c) Sampling sites for Tingming Lake. The red star represents the location of sediment core 17TM3, and the blue and red dots represent the locations of surface soils and surface sediments, respectively.

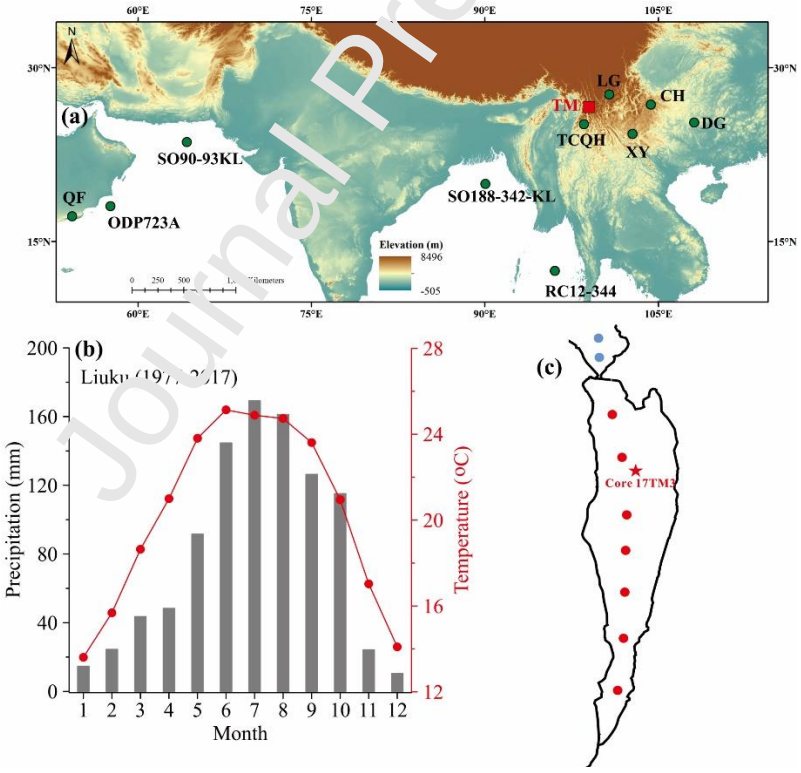

Figure. 2 Average *n*-alkane distributions in (a) plants, (b) surface soils, (c) surface sediments and (d) core sediments of Tingming Lake. Relative abundance of isoGDGTs in (e) core samples, surface sediments and surface soils.

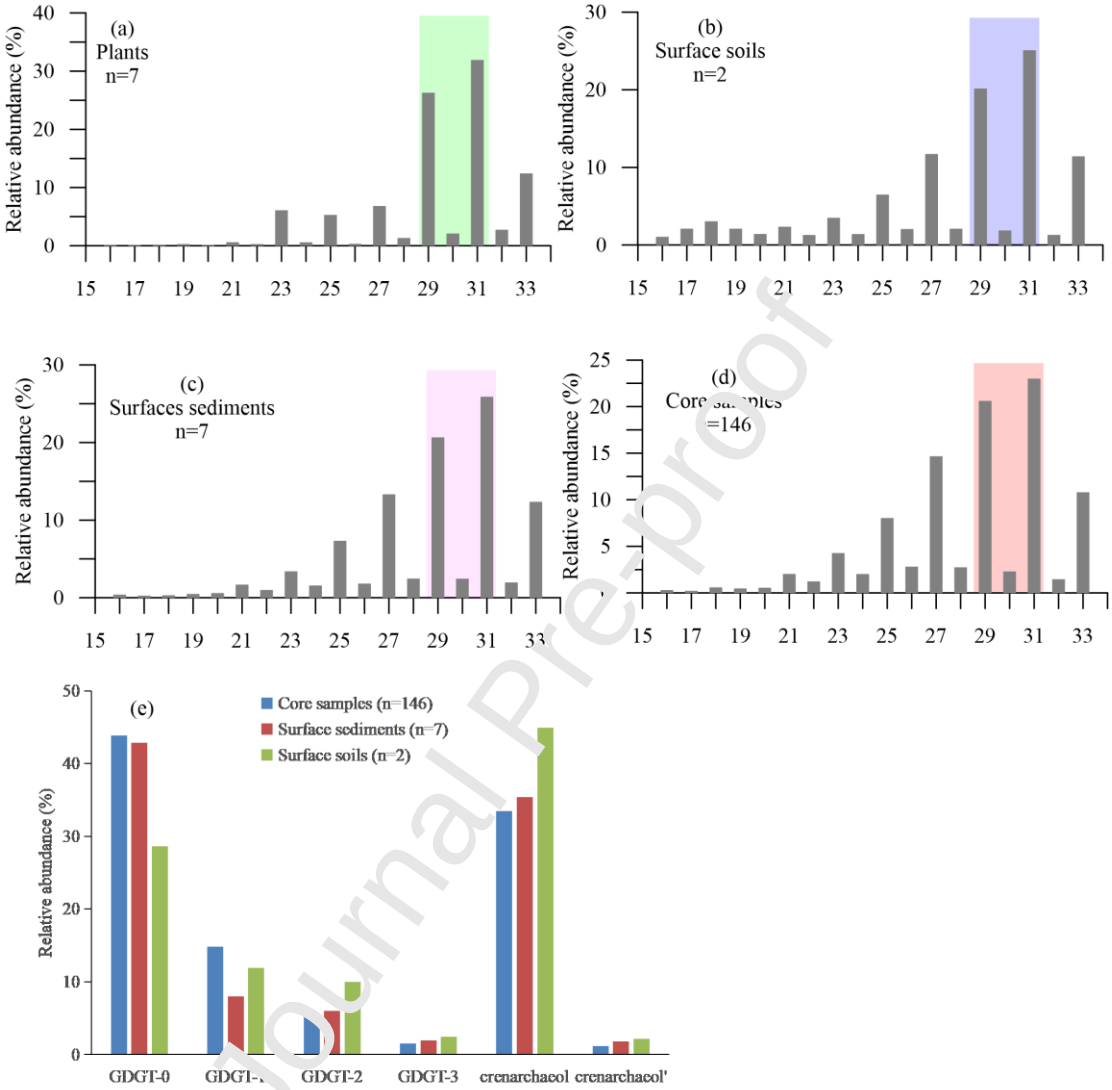

Figure. 3 Various *n*-alkane-based proxies for Tingming Lake. (a) ACL, (b) C_{31}-C_{33} (%), (c) methane index. The gray bar implies the YD event.

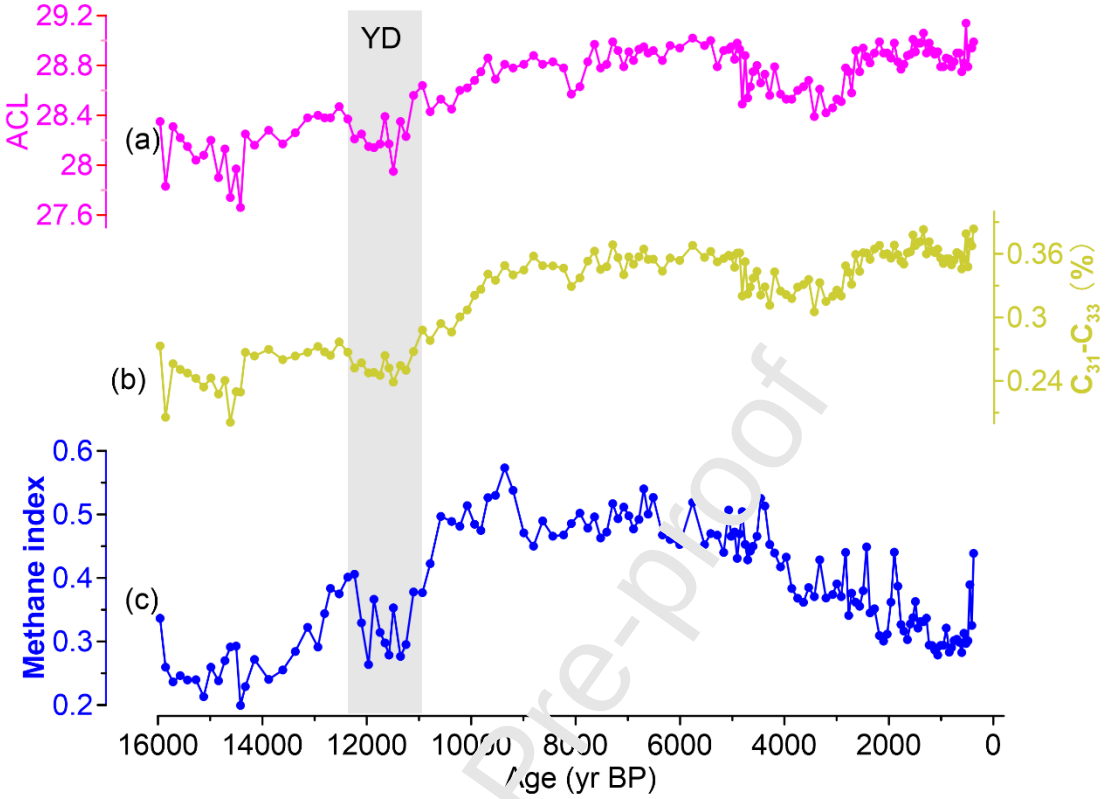

Figure. 4 Correlations between the methane index and lake water depth of Tingming Lake (blue), Gonghai Lake (green, Cao et al., 2021) and Fuxian Lake (orange, Zheng et al., 2022). R^2 represents the correlation coefficient.

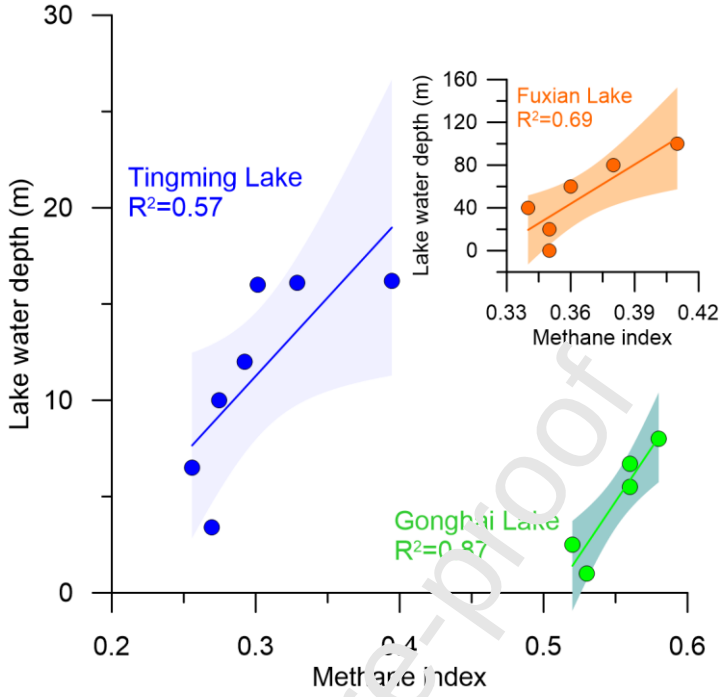

Figure. 5 Comparison of (h) effective humidity record from Tingming Lake (this study) with (a) mean annual precipitation reconstructed from Tengchongqinghai Lake and Caohai Lake (Zhang et al., 2023c); (b) stalagmite $\delta^{18}O$ records from Dongge Cave (Dykoski et al., 2005; Wang et al. 2005); (c) stalagmite $\delta^{18}O$ record from Qunf Cave (Fleitmann et al. 2003); (d) leaf wax δD from Lugu Lake (Zhao et al., 2021b); (e) carbonate $\delta^{18}O$ record from Xingyun Lake (Wu et al., 2018); (f) δD_{wax} record from core SO188-342 KL in the northern Bay of Bengal (Contreras Rosales et al., 2014); (g) surface-water $\delta^{18}O$ data for sea-surface salinity reconstructions from core RC12-344 (Rashid et al., 2007).

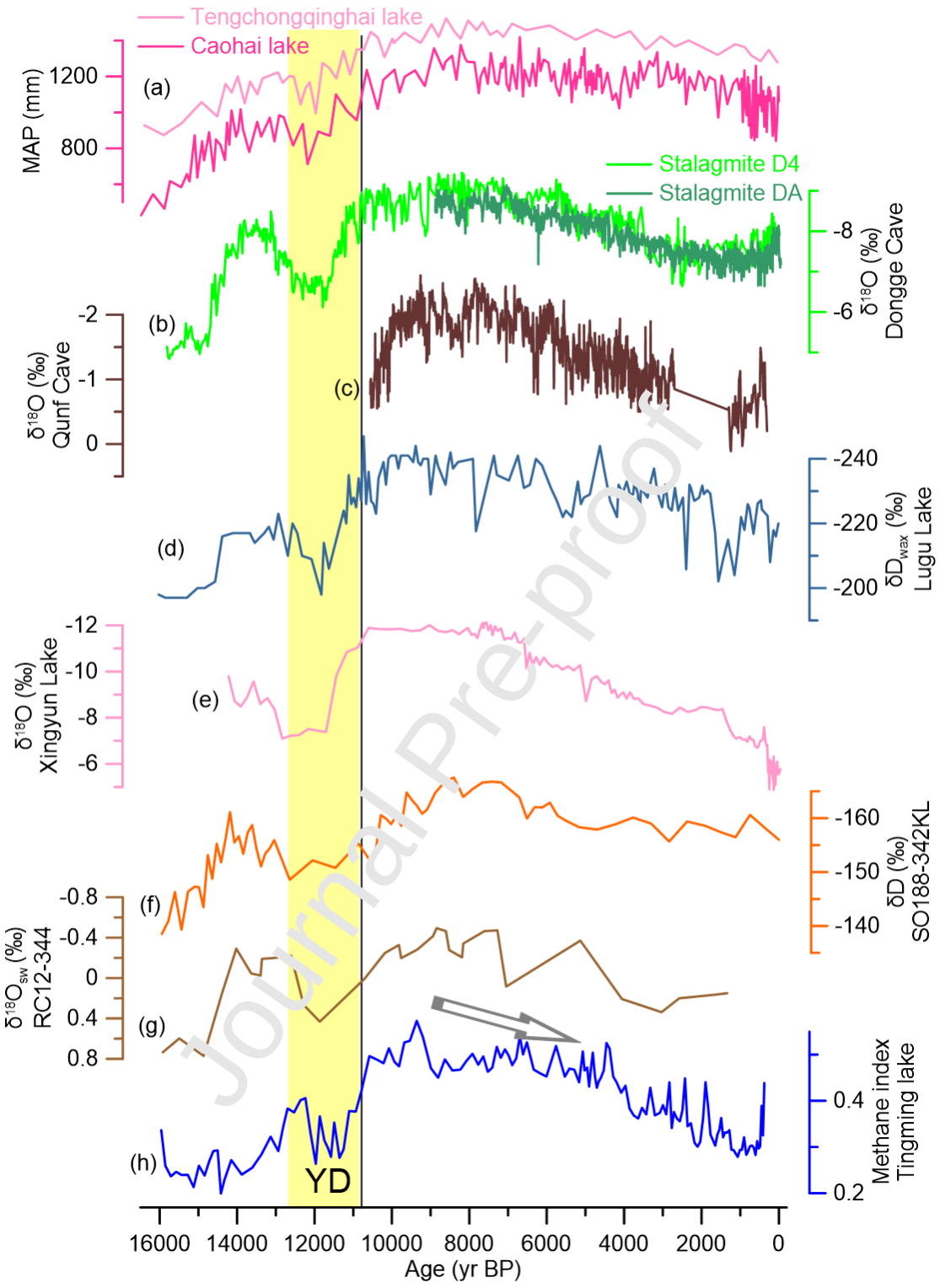

Figure. 6 Deglaciation and Holocene reconstructed temperature in this study compared with other palaeotemperature records in southwestern China. (a) Stacked annual temperature anomaly (Zhang et al., 2022); (b) alkane ACL of Tingming Lake (this study); (c) MAAT of Tengchongqinghai Lake (Zhao et al., 2021a); (d) MAAT of Lugu Lake (Zhao et al., 2021a); (e) stacked summer temperature anomaly (Zhang et al., 2022); (f) summer temperature of Tiancai Lake (Zhang et al., 2017a, 2019b); (g) summer temperature of Qinghai Lake (Hou et al., 2016).

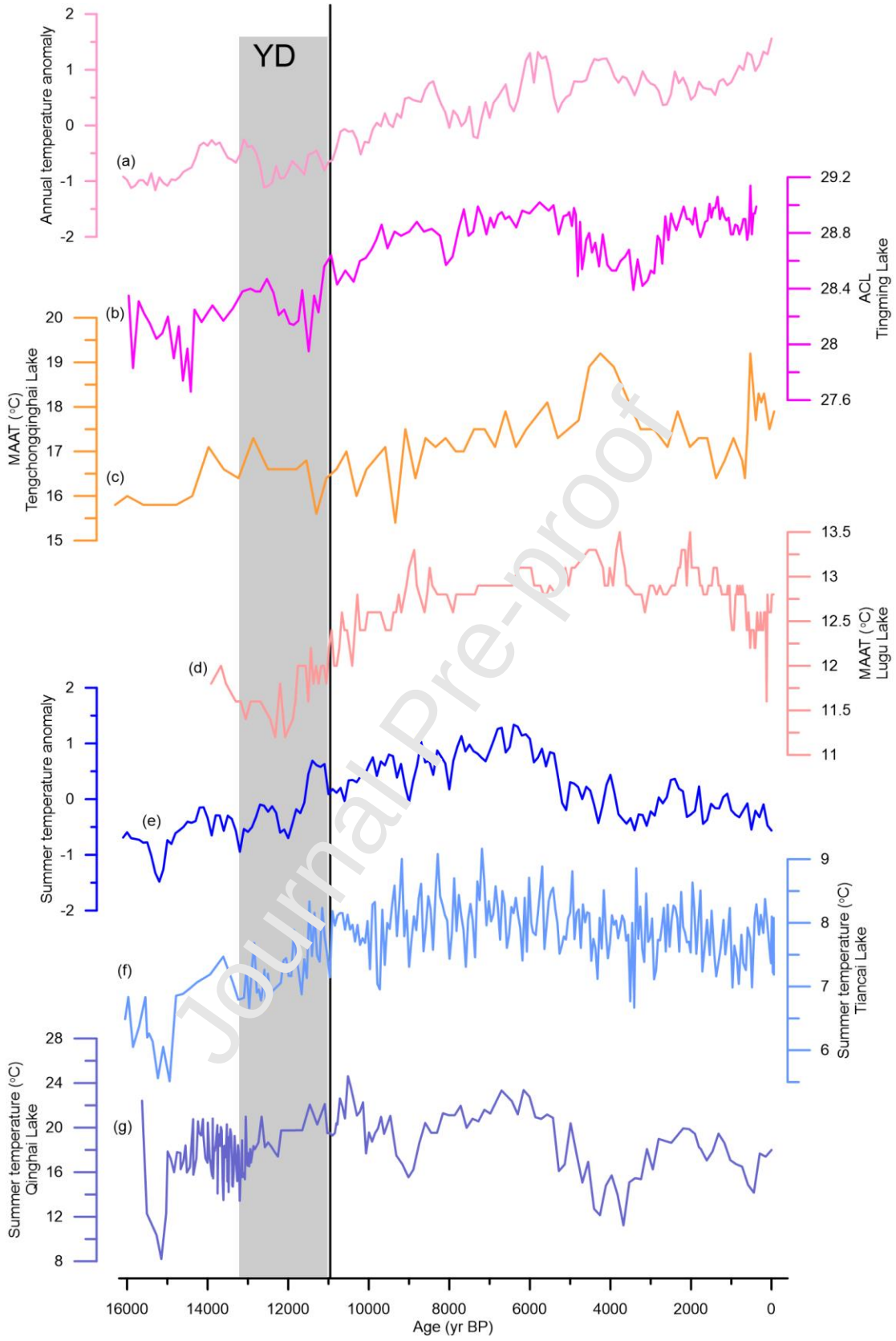

Figure. 7 Correlations of reconstructed temperature with other climate records. (a) Alkane ACL in Tingming Lake (this study), stacked annual temperature (Zhang et al., 2022); (b) stacked summer temperature anomaly (Zhang et al., 2022); (c) MAP (Zhang et al., 2023c) and methane index from Tingming Lake (this study); (d) δD_{wax} of Lugu Lake (Zhao et al., 2021b) and $\delta^{18}O$ of Dongge Cave (Dykoski et al., 2005); (e) SST for SO90-93KL (Böll et al., 2015) and ODP723A (Naidu et al., 2005) from the Indian Ocean; (f) Ti content from the Cariaco Basin (Haug et al., 2001); (g) CO_2 concentration from the Dome C ice core (Lüthi et al., 2008); (h) insolation anomaly (Laskar et al., 2004).

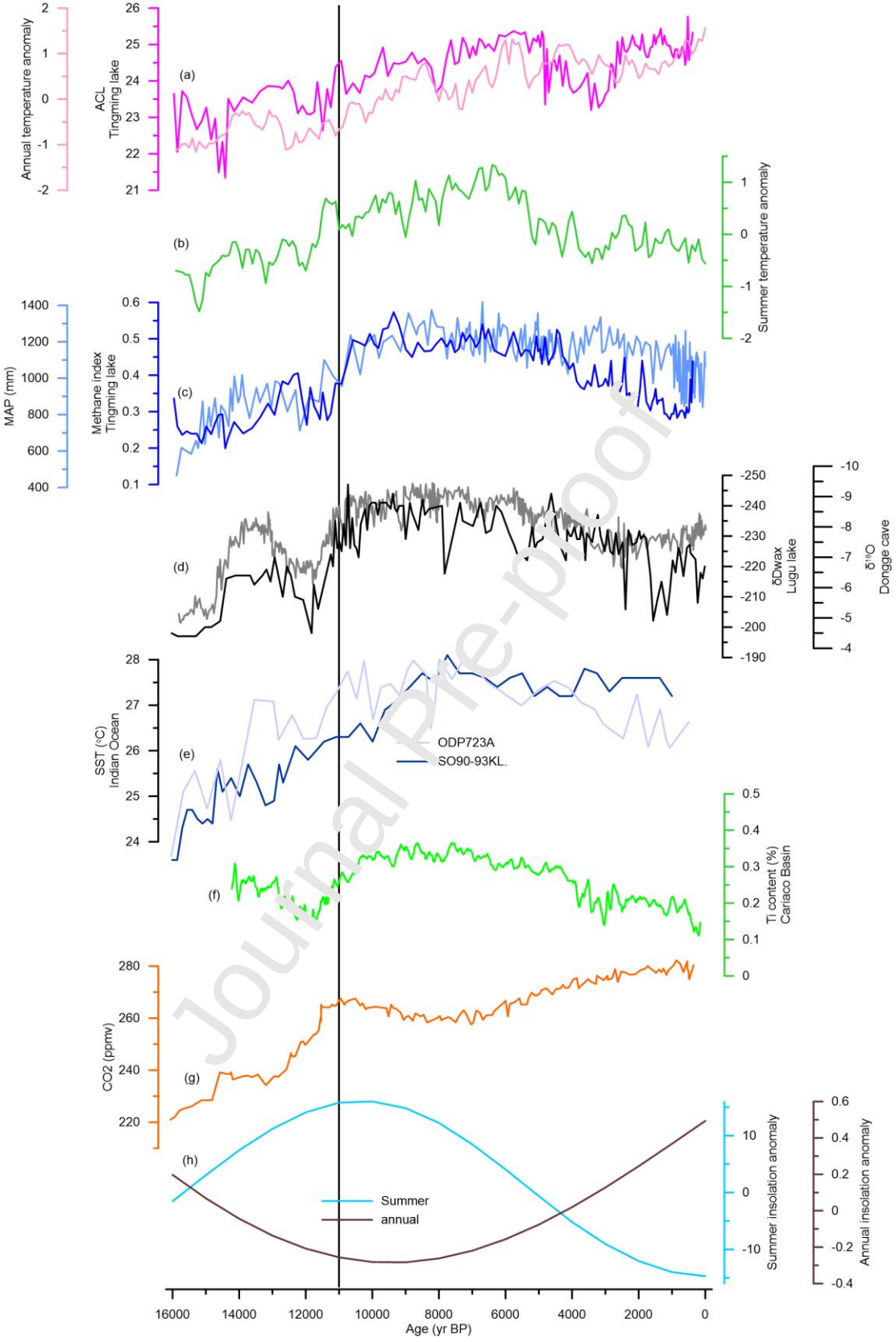

Conflict of Interest:

The authors declare that they have no known competing financial interests.

Highlights:

- Our reconstructed monsoon precipitation and mean annual temperature synchronously increase during the deglaciation.
- Monsoon precipitation shows a general decline during the Holocene while an overall increase for mean annual temperature.
- Monsoon precipitation is primarily driven by summer insolation, while the mean annual temperature is mainly affected by greenhouse gases during the deglaciation and by local annual insolation in the Holocene.
- Monsoon precipitation is a summer signature, consistent with summer temperature changes but contrasting with mean annual temperature changes.